#141 Dupl

FERMILAB-PUB-73-146-E

#141 PRL

ANL/HEP 7356
November 8, 1973

Diffraction Dissociation in Four-Prong Proton-Proton Interactions at 205 GeV/c*

M. DERRICK, B. MUSGRAVE, P. SCHREINER,
P. F. SCHULTZ and H. YUTA

Argonne National Laboratory, Argonne, Illinois 60439

We analyze the diffraction process in four-prong pp interactions at 205 GeV/c. The $p\pi^+\pi^-$ state contributes only 25% to the proton dissociation and, as observed for momenta below 30 GeV/c, this state is confined to masses $\lesssim$ 3 GeV. Substantial excitation occurs into states involving three or more pions and with masses as high as 7 GeV. Isovector exchange background is small, as studied using the missing mass of the system recoiling from a prominent Δ^{++} state.

*Work supported by the U. S. Atomic Energy Commission.

Recent studies of inclusive proton-proton (pp) collisions reveal a broad, low-mass enhancement produced peripherally from either the target or projectile proton.[1] Since the production cross section of this enhancement is approximately constant, at about 6 mb, from 100 to 1500 GeV/c, it has been interpreted as diffractive breakup of the proton. Nothing is known about the exclusive contributions to the enhancement or about its relationship to lower energy phenomena such as the $N^*(1470)$ resonance although the dominant contributions to the peak occur for the two- and four-prong events with a small contribution from the six-prong topology.[2, 3]

Our study of the low-mass enhancement utilizes complete measurements of four-prong events in 50, 000 pictures of the 30-inch bubble chamber exposed to 205 GeV/c protons at the National Accelerator Laboratory. The sample of 1191 events used for physics analysis comprises 95% of the four-prong events; the remaining 5% do not affect our conclusions.

The histogram in Fig. 1(a) shows the distribution of missing mass squared (MM^2) for the system recoiling off identified protons with laboratory momentum < 1.5 GeV/c. Referring to events with i charged particles in the forward and j in the backward CM hemisphere as "(i, j) events," the shaded area of Fig. 1(a) corresponds to (3, 1) events; also shown cross-hatched are the (2, 2) events. We note: (a) most of the low-mass enhancement, and particularly the prominent peak appearing for $MM^2 < 10$ GeV^2, is associated with the (3, 1) events, (b) the (2, 2) events make a small

contribution for $MM^2 \leq 50\ GeV^2$, mostly concentrated between 20 and 50 GeV^2 and (c) the remaining events, (1, 3) and (0, 4), have a structureless distribution. The events in Fig. 1(a) with $MM^2 \leq 50\ GeV^2$ give a cross section of 1.55 ± 0.09 mb; 1.09 ± 0.08 mb of this corresponds to the (3, 1) events. These and subsequent cross sections are quoted for one CM hemisphere.

The four-prong topological cross section of 5.91 ± 0.28 mb can be separated into parts with only 0, 1, 2, 3 or 4 charged particles in the forward CM hemisphere. These cross sections are 0.19 ± 0.03, 1.89 ± 0.10, 1.66 ± 0.10, 1.97 ± 0.10 and 0.19 ± 0.03 mb, respectively. The preference for a three-to-one partition of the charged particles can be identified with the predominance of (3, 1) events in the low-mass enhancement of Fig. 1(a).

Next we discuss the rapidity structures of the events using the pseudorapidity $\eta = \ln \tan(\theta/2)$, where θ is the laboratory space angle between a secondary track and the beam track. Singly diffractive events should show a large gap in the ordered rapidity chain of the secondary particles, separating the leading particle from the diffractive cluster. The 219 (3, 1) events in Fig. 1(a) with $MM^2 \leq 50\ GeV^2$ have an average rapidity gap of four between the recoil proton and its nearest neighbor, and for all of these events, this first gap is the largest. The three forward hemisphere particles form a cluster with a spread in rapidity of ± 1. For the 69 (2, 2) events with $MM^2 \leq 50\ GeV^2$, however, the average gap between the recoil proton and its nearest neighbor is about 2.2 and for only 31 events is this gap the largest.

The middle gap is largest for 16 events.[4] We conclude that the (2, 2) events are not predominantly diffractive.

Defining as diffractive those events having both $MM^2 \leq 50\ GeV^2$ and a rapidity gap ≥ 2.5 between the leading proton and its closest neighbor, we obtain a four-prong single-diffractive cross section of 1.19 ± 0.08 mb.[5]

We now proceed to determine how often the excitation results in particle multiplicity higher than the $N\pi\pi$ observed for the N^*(1470, 1520, ----) resonances diffractively produced at lower beam energies. In a separate analysis of the four-prong events considered here, we find the reaction

$$pp \rightarrow pp\pi^+\pi^- \qquad (1)$$

is dominated by proton dissociation into $p\pi^+\pi^-$.[6] Events belong predominantly, about 90%, to the (1, 3) or (3, 1) categories. The cross section for those events of reaction (1), which satisfy our definition of single diffraction, is 0.32 ± 0.07 mb out of a total one hemisphere cross section of 0.34 ± 0.07 mb.

Fig. 1(b) shows the distribution of MM^2 for the (3, 1) events of reaction (1). The contribution from the $p\pi^+\pi^-$ state is confined to the <u>low-mass part</u> of the diffractive peak in Fig. 1(a). These distributions may be compared to the MM^2 distribution for the two-prong events with an identified proton in this exposure,[2, 7] Fig. 1(c). Not only does the peak position occur at a lower mass in Fig. 1(c) than for Fig. 1(a), but it is also lower than for the $p\pi^+\pi^-$ system in Fig. 1(b). This observation suggests a

large part of the diffractive enhancement in the two-prong events goes through the $N\pi$ state.

Next we estimate the separate contributions of $p\pi^+\pi^-\ell\pi^0$ ($\ell \geq 1$) and $n\pi^+\pi^+\pi^-m\pi^0$ ($m \geq 0$) to the single diffractive cross section. The MM^2 distribution corresponding to these states is shown in Fig. 1(d) and is simply obtained by subtracting from the diffractive component of Fig. 1(a) those events assigned to the $pp\pi^+\pi^-$ final state. One sees a much broader distribution shifted to higher mass when the $pp\pi^+\pi^-$ events are excluded. We now use the events which, in the overall CM system, are symmetric to those in Fig. 1(d), and where again we can utilize our ability to identify slow particles. To select the symmetric events, we use Fig. 2 which shows a scatter plot of either the largest or the smallest η in an event versus the η gap from its closest neighbor. For each event we plot only the combination where the gap is the largest. All events except those assigned to reaction (1) are included, but the two enclosures indicate where those events would fall. In fact, the right-hand enclosure also isolates the diffractive events in Fig. 1(d), together with a small (~ 15%) background, mainly from double diffractive processes. The desired symmetric events which we use are, therefore, in the left-hand enclosure.

Fig. 1(e) shows the $p\pi^+\pi^-$ effective mass squared distribution for events selected as above and where the proton is identified. A peak is observed but shifted to lower mass than for the projectile dissociation

enhancement, Fig. 1(d), as a result of not including π^o's when calculating the effective mass.[8] We estimate from Fig. 1(c) that 0.39 ± 0.06 mb of diffractive production comes from the final states $p\pi^+\pi^-\ell\pi^o$. Since proton identification is required, this result represents a lower limit to the contribution.

About 9% of the four-prong events have two slow positive particles that were identified by ionization to be pions. Of these, there is a clearly separated group which falls within the left-hand enclosure, corresponding to a cross section of 0.14 ± 0.03 mb. This clustering of two π^+ and an assumed π^- clearly separated from a leading particle shows diffractive production of the $n\pi^+\pi^+\pi^-m\pi^o$ states, and the quoted cross section again represents a lower limit.

The remaining diffractive events, corresponding to a cross section of 0.24 ± 0.04 mb, could not be assigned to the neutron or proton final states above because of lack of particle identification.

We conclude that the nucleon plus three or more pion states contribute to the diffractive excitation, in agreement with the evidence from the six-prong events.[2, 3]

Both isoscaler and isovector exchange processes may contribute to the low-mass enhancement discussed above. To study the production of such a peak by I = 1 exchange, we use the events with an identified Δ^{++}. Fig. 3(a) shows the $p\pi^+$ effective mass plot for the two- and four-prong events that

have two low-momentum positive particles;[9] the two-prong events are shown hatched. Two-thirds of the Δ^{++} peak is associated with the (1, 3) diffractive enhancement, and these Δ^{++} are decay fragments of diffractively produced states. Defining the Δ^{++} as $p\pi^+$ mass $\leq$ 1.32 GeV, the distribution in missing-mass-squared recoiling from the Δ^{++} is shown in Fig. 3(b). The shaded four-prong events have the additional selection η gap $\geq$ 2.5 and exhibit a small low-mass peak as might be expected for such a selection. Applying our criteria for diffractive production, we obtain a cross section of 0.084 ± 0.020 mb compared to 1.19 ± 0.08 mb for the proton case. This strongly suggests that only a small part of the low mass peak of Fig. 1(a) can come from isovector exchange.

References

1. "Experiments on High Energy Particle Collisions 1973," Edited by R. S. Panvini, AIP Conference Proceedings, No. 12 contains a recent summary of the data.

2. S. J. Barish et al., Phys. Rev. Letters 31, 1080 (1973) contains an analysis of all events with a slow proton in this exposure using measurements of only the beam and the proton tracks.

3. F. T. Dao et al., Phys. Letters 45B, 339 (1973).

4. The existence of a large rapidity gap does not by itself guarantee a diffractive event. Thus, for all four-prong events we find 230 cases

where the middle rapidity gap is the largest gap and is sometimes as large as four. Charge transfer must occur across this gap.

5. The result obtained using our definition of diffraction is in good agreement with the value 1.20 ± 0.19 mb of Barish et al. (Ref. 2), obtained from an analysis of the MM^2 peak.

6. M. Derrick et al., ANL/HEP 7354, submitted to Phys. Rev. D1, October 1973.

7. S. Barish et al., ANL/HEP 7337, submitted to Phys. Rev. D1, October 1973.

8. The difference in resolution of the MM^2 and the $p\pi^+\pi^-$ effective mass does not affect this conclusion.

9. F. T. Dao et al., Phys. Rev. Letters 30, 34 (1973) have studied inclusive Δ^{++} production in 303 GeV/c pp interactions.

Figure Captions

Fig. 1 The distribution in MM^2 from the identified proton: (a) for all four-prong events. There are 224 events overflow. The (3, 1) events are shown shaded; the (2, 2) events are cross-hatched; (b) for the $pp\pi^+\pi^-$ final state where the $p\pi^+\pi^-$ system is in the forward CM hemisphere; (c) for the two-prong events with an identified proton; (d) for the singly diffractive events in (a) above but

with events assigned to the reaction $pp \rightarrow pp\pi^+\pi^-$ removed, and (e) the squared effective mass distribution of the $p\pi^+\pi^-$ system for the events symmetric in the CM system to those events in (d) above which satisfy the criteria for single diffraction in the text.

Fig. 2 Scatter diagram of the η, which is either the largest or smallest in the ordered rapidity chain of the four-charged particles, versus the rapidity gap to the nearest neighbor. The $pp \rightarrow pp\pi^+\pi^-$ events have been removed. Each event appears once using the pair of variables with the largest rapidity gap.

Fig. 3 For two- and four-prong events with an identified proton and π^+: (a) the effective mass of the $p\pi^+$ system. The cross-hatched events are two-prong events and (b) the MM^2 distribution for the system recoiling from the $\Delta^{++}(1236)$. The cross-hatched events are the two-prongs and the shaded events have a rapidity gap of $\geqslant 2.5$ between the Δ^{++} and its nearest neighbor.

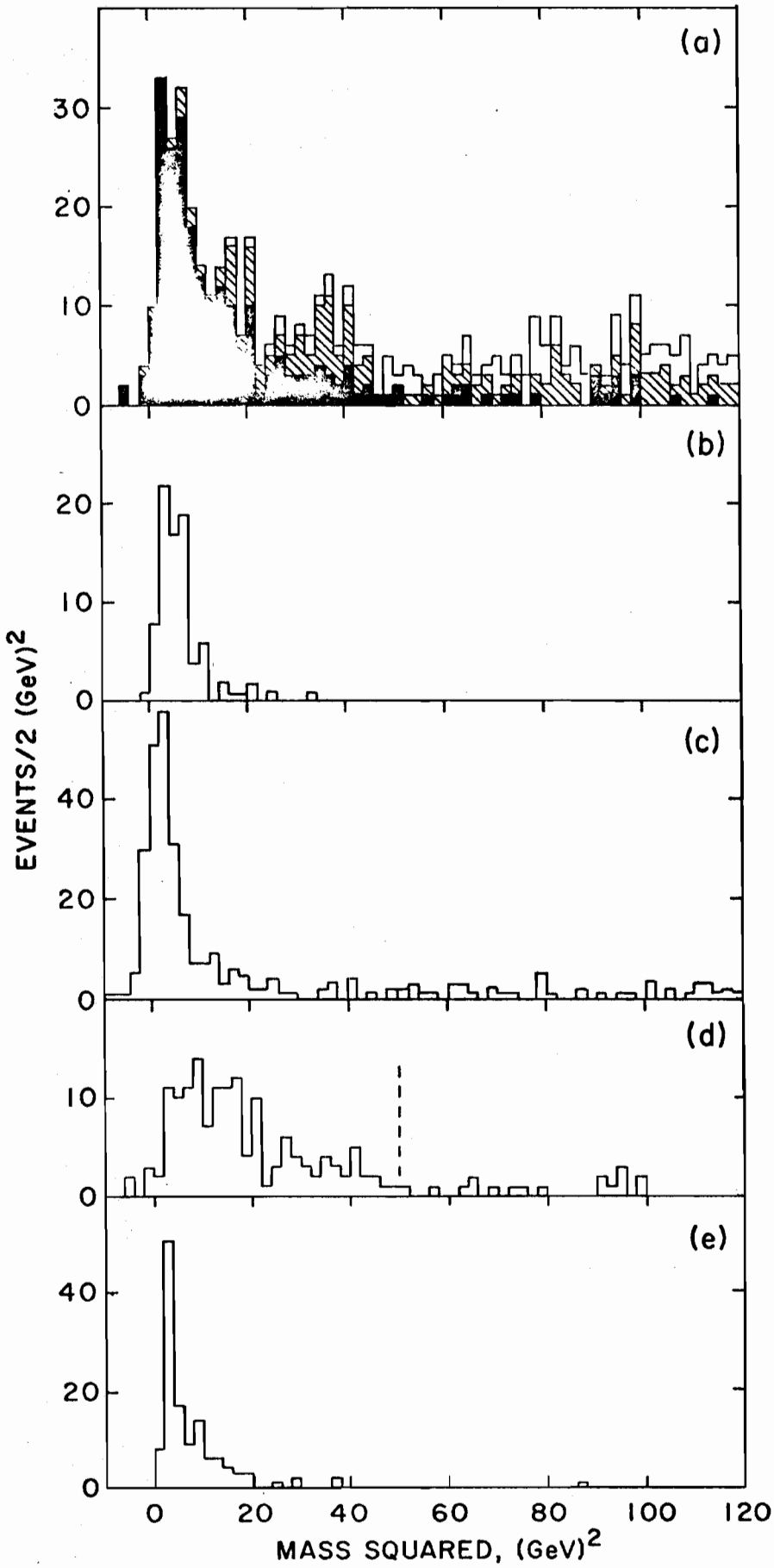

Fig. 1

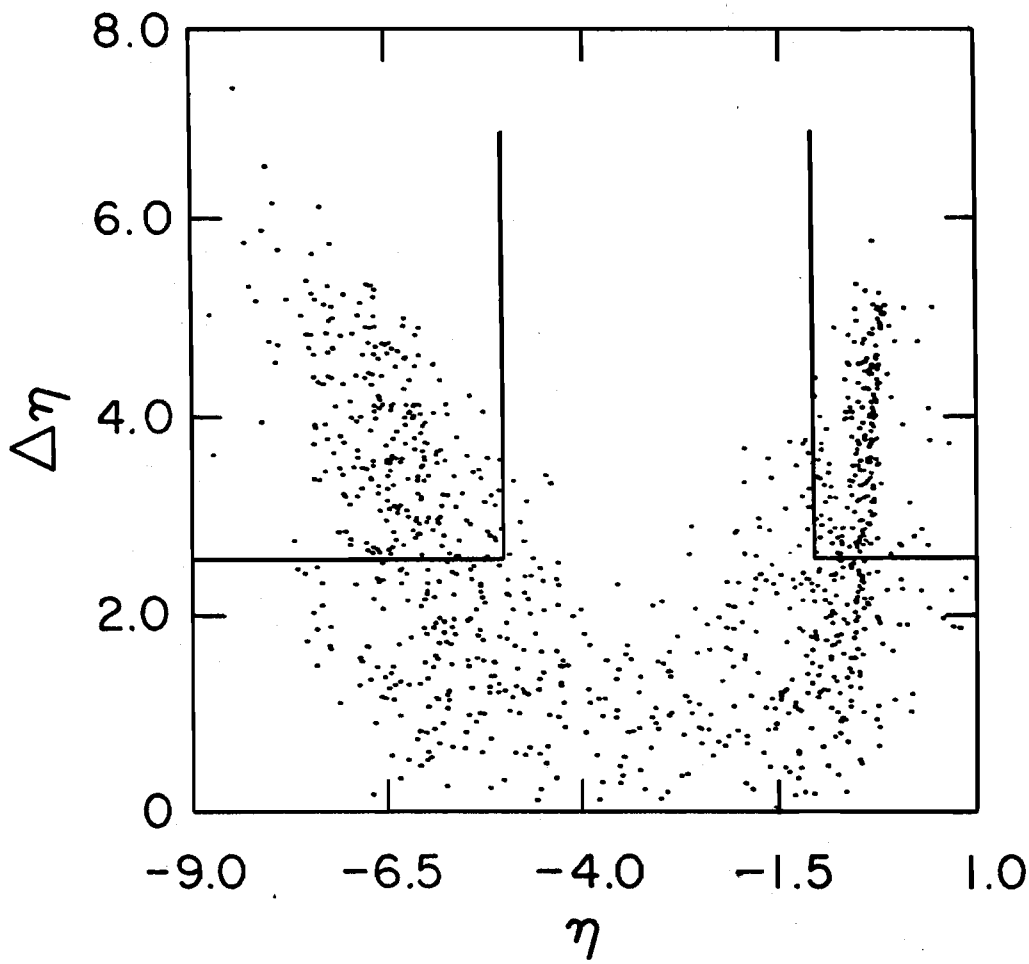

Fig. 2

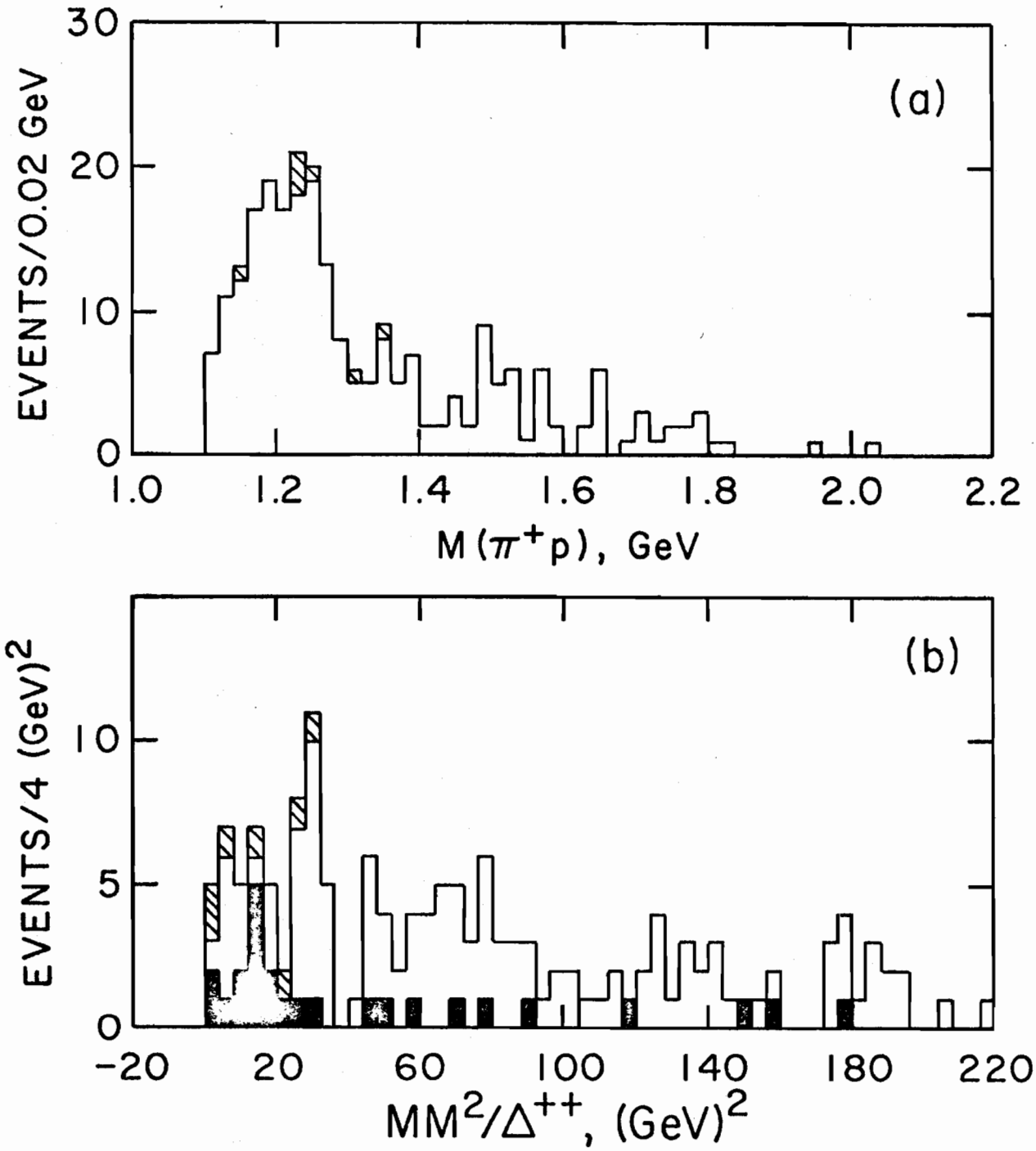
(a)
EVENTS/0.02 GeV
30
20
10
0
1.0
1.2
1.4
1.6
1.8
2.0
2.2
M(π⁺p), GeV
(b)
EVENTS/4 (GeV)²
10
5
0
-20
20
60
100
140
180
220
MM²/Δ⁺⁺, (GeV)²

Fig. 3